

On-Line Gradient Based Surface Discontinuity Detection for Outdoor Scanning Range Sensors

Martin D. Adams

School of Electrical & Electronic Engineering
Nanyang Technological University, Singapore.
email: eadams@ntu.edu.sg

Abstract

Research in field robotics often utilises scanning range sensors to aid autonomous navigation. This article addresses reliable feature extraction from continuously scanning range sensors operating outdoors. Contrary to other detection methods, an algorithm is presented which detects features on-line, as soon as the range to that feature has been sensed. A model is derived which makes predictions of range, before each new range sample is recorded. These are used to produce validation regions within which each new sample should lie, provided it belongs to the surface with the same smoothness characteristics as its range predecessors. The detection process model adapts its validation region according to the spatial gradient of the surface being sensed, and is implemented in extended Kalman Filter (EKF) recursive form. Results are demonstrated with laser detection and ranging (ladar) sensor data recorded outdoors.

1 Introduction

An extremely useful asset to aid autonomous robot navigation is the estimation of range. Recent research in rugged, outdoor environments has exploited mm-wave radar and laser detection and ranging (ladar) technologies, while sensing methods for the detection of sea floor features also include scanning coherent illumination and side-scan sonar methods [1, 2, 3]. There is also a trend in vehicle localization research which uses scanning range finders as an aid to vision based methods for feature detection [4].

To solve the localization problem, some part of a sensor scan must be discernible from all other parts, and must be possible to find again from sensor data recorded in other locations. Such data corresponds to a “feature”. This article focuses on the reliable extraction of such features from continuously scanned range data. It will be demonstrated that a chosen type of feature must have a strictly defined mathematical method for its identification, which guarantees its future identification, when scanned from other locations. Only then can feature matching and autonomous localization and map building take place [5]. Section 2 reviews some of the feature detection algorithms applied to vehicle navigation and examines the advantages of a planar surface edge de-

tection algorithm, previously published by the author, when applied to continuously scanning range finders. In the outdoor or under water world, the presence of planar surfaces cannot be assumed. Therefore an algorithm is presented in section 2 which is still optimally suited to process continuously scanned range data, but will generalize the features it finds to any kind of surface in which changes in “smoothness” occur.

Some initial results in estimating the change in spatial gradient of various surfaces will be given in section 3.

To optimize the performance of a feature detector based on the changes in gradients along a scanned surface, section 4 uses this quantity to derive range bounds for the next range point. This is done under a recursive, extended Kalman filter (EKF), discrete time, state update formulation.

Finally section 5 shows results of the feature detector running on real ladar range data recorded outdoors, and demonstrates the potential for successfully matching detected features, from differing sensor positions.

2 On-Line Feature Detection

While a great deal of research has been published on the extraction of image discontinuities in vision, the robust detection of features from range data is less publicized. The extraction of regions of constant depth from sonar data, which can be used to detect walls and corners is a successful technique, but requires the collection of large volumes of data, from different vehicle positions [5]. Use of the Hough Transform has been applied to optical range data in order to extract line segments from noisy data [6]. In all of these methods, features are extracted only after a complete scan is made and no account of unique range variances associated with the range data is made.

This article extends previous work published by the author to the general detection of changes in “smoothness” of any arbitrary surface, as an on-line process [7]. Consider, for example, the general planar surface shown in figure 1 and the corresponding sensed data points which would result from a perfect scanning line of sight sensor. Simple trigonometry shows that the relationship between successive range readings, when the light beam

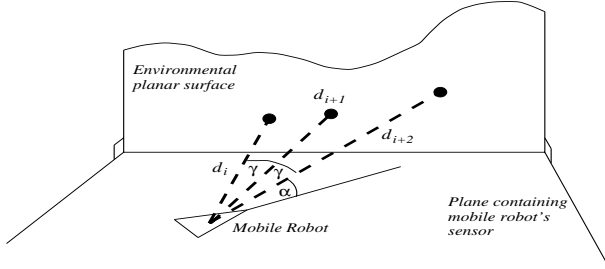


Figure 1: The relationship between successive range readings when scanning a planar surface.

is incident upon a planar surface is:

$$d_{i+2} = \frac{d_i d_{i+1}}{(2d_i \cos \gamma) - d_{i+1}} \quad (1)$$

where γ is the constant angle (in bearing) between successive samples of the sensor as it rotates about its vertical axis. Note that the relationship given in equation 1 is *independent* of the elevation angle α .

Equation 1 is a second order difference equation with respect to time since range sample d_{i+2} is recorded one time unit after d_{i+1} . Even though only two points are necessary to provide the predicted third point, by defining two states, the system can be completely defined by a 2D discrete time difference equation, lending itself to a recursive, Kalman filter estimation process. This technique is used to validate range observations with their expected values, which are optimized with respect to sensor noise and the above model. Hence observations which could not be validated were considered no longer to belong to the planar surface, which was being tracked, and were marked as edges.

This system model has provided a good basis for edge detection within indoor environments, but in the outdoor world, the assumption that planar surfaces exist, becomes rather restrictive. While it is useful to keep the on-line nature of the above discontinuity detection algorithm, the planar surface model will now be changed.

As a result of analyzing laser detection and ranging (ladar) scans in various environments, such as car parks, dense tropical jungle and rocky cliff faces, it has been noted that monitoring changes in spatial gradient can be used to detect features reliably¹ [8]. This time however, *two* possible values for the next predicted range reading will result based on the expected change in gradient, in a positive or negative sense. In particular, once the first two points are sensed, a local coordinate system in the sensor space (x_s, y_s) can be defined as shown in figure 2. The x_s axis is the line joining both end points of d_i and

¹Since the changes in range itself becomes so pronounced at the extremities, one may ask why not just monitor these changes to find the edges? The problem here is, that when the sensor line-of-sight subtends a large angle of incidence with the surface normal (near tangential scanning), large changes in range are to

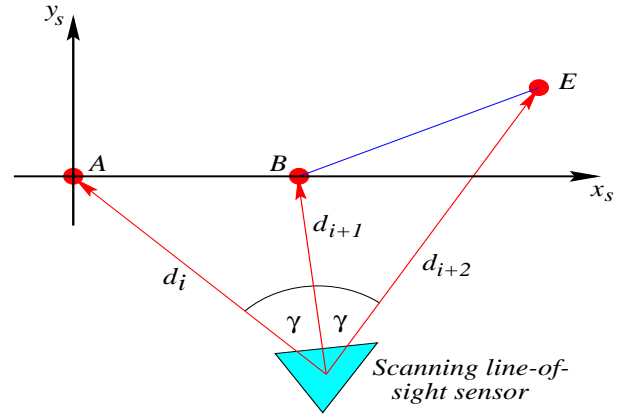


Figure 2: Three successive range points, d_i , d_{i+1} and d_{i+2} are recorded sequentially in time and space, separated in space by a constant incrementing angle γ . The local coordinate system is defined such that the x_s axis connects the first 2 range points A and B.

d_{i+1} , and clearly in this coordinate system the gradient of line AB is zero. Without loss of generality, the change in gradient between AB and BE is the gradient of BE, which can be determined as a function of d_i , d_{i+1} , d_{i+2} and γ :

$$\Delta \left. \frac{dy_s}{dx_s} \right|_{x_s=B} = \frac{(d_i d_{i+1} + d_{i+1} d_{i+2} - 2d_i d_{i+2} \cos \gamma) \sin \gamma}{d_{i+1}^2 - d_i d_{i+1} \cos \gamma - d_{i+1} d_{i+2} \cos \gamma + d_i d_{i+2} \cos 2\gamma}$$

It should be noted that this is the change in gradient between AB and BE in *any* chosen coordinate system — a necessity for matching techniques, when the same feature is searched from different positions.

3 Real and Simulated Data

The use of the above equation is analyzed in figures 3 to 5, where plots of actual range and $\Delta \frac{dy_s}{dx_s}$ versus scanning angle are shown, for various sensed objects.

Initially the graphs in figures 4 and 5 were recorded using a prototype scanning ladar, adapted for outdoor use [7]. The spatial differential $\Delta \frac{dy_s}{dx_s}$ of the signal is numerically determined in the lower graphs of each figure, which is well known to be greatly affected by noise [9]. To separate the geometrical effect from the measurement noise effect on $\Delta \frac{dy_s}{dx_s}$, the range data was also simulated in each case, by hand measuring the geometry of the scanned surfaces with respect to the sensor's position. The graphs in figure 3 show the results which would be obtained with a noiseless, perfect line-of-sight scanning sensor, when sensing the wall. The edges of

be expected even when no extremity is being sensed.

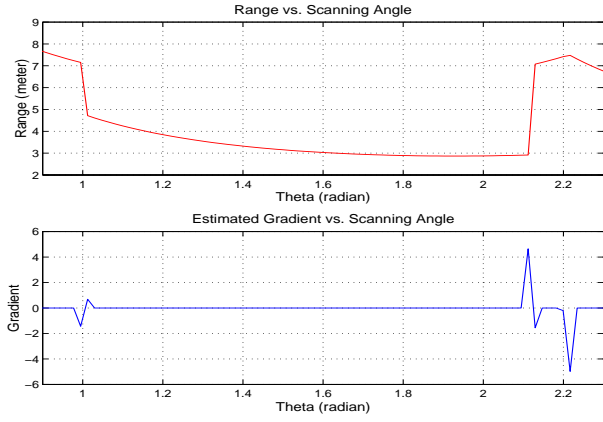


Figure 3: Simulated line-of-sight data and $\Delta \frac{dy_s}{dx_s}$ versus scanning angle as the sensor scans a wall.

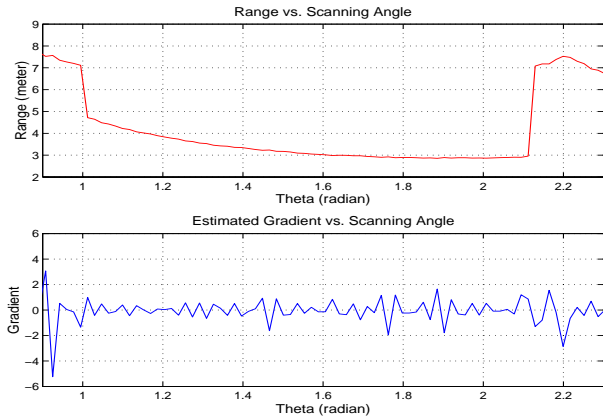


Figure 4: Recorded line-of-sight data and $\Delta \frac{dy_s}{dx_s}$ versus scanning angle as the sensor scans a wall.

the wall are clearly discernible from the peaks in the gradient. With the real measurements (figure 4), these peaks must be determined amongst those resulting from sensor measurement noise.

In the real data recorded from the rock surface (figure 5), noise corrupts the magnitudes of the estimated gradients, however close examination of the lower graph in figure 5 shows marked increases in the gradient at the edges, and at other points along the surface. Clearly range estimation noise must be dealt with in the recursive estimation of features, and will be covered in section 4.2.

4 Prediction of Range Bounds

From the estimate of $\Delta \frac{dy_s}{dx_s}$, a *minimum* value for the next range reading d_{i+3}^- is predicted, based on the next spatial gradient changing by $-\Delta \frac{dy_s}{dx_s}$, and a *maximum* value d_{i+3}^+ is predicted based on the next gradient changing by $+\Delta \frac{dy_s}{dx_s}$. This is demonstrated in figure 6. From

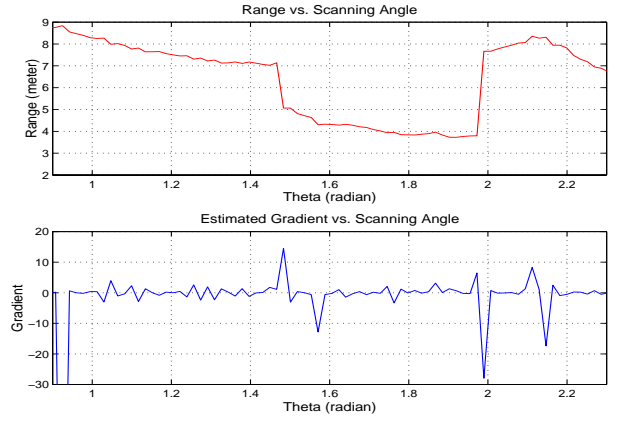


Figure 5: Recorded line-of-sight data and $\Delta \frac{dy_s}{dx_s}$ versus scanning angle as the sensor scans a rocky cliff face.

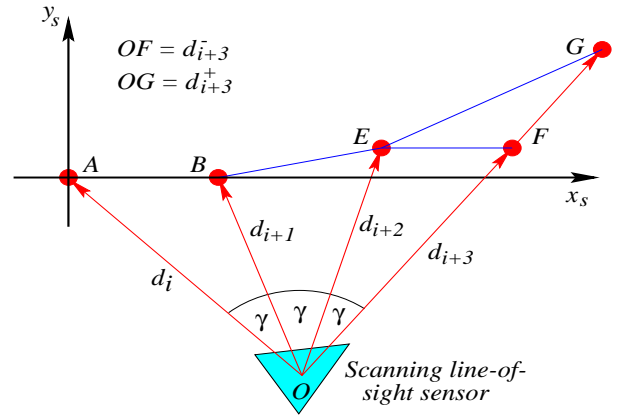


Figure 6: Predicted bounds for range reading d_{i+3} (FG), based on a negative or positive change in gradient equal in magnitude to the previous change (gradient BE).

the figure it can be shown that:

$$\begin{aligned} d_{i+3}^- &= f^-(d_i, d_{i+1}, d_{i+2}, \gamma) \\ &= \frac{(2d_i - d_{i+1})d_{i+2}}{d_i - 2d_{i+1} \cos \gamma + 2d_i \cos 2\gamma} \end{aligned} \quad (2)$$

and:

$$\begin{aligned} d_{i+3}^+ &= f^+(d_i, d_{i+1}, d_{i+2}, \gamma) \\ &= d_{i+3}^- + \frac{2d_{i+2}(d_i^2 + d_{i+1}^2 - 2d_i d_{i+1} \cos \gamma)}{(d_i - 2d_{i+1} \cos \gamma + 2d_i \cos 2\gamma)} \\ &\quad \times \frac{(2d_i d_{i+2} \cos \gamma - d_i d_{i+1} - d_{i+1} d_{i+2})}{(R + S + T + U)} \end{aligned} \quad (3)$$

where R, S, T and U are functions of d_i, d_{i+1}, d_{i+2} and γ .

4.1 Discrete Time System Model

To form a true recursive prediction formula, equations 2 and 3 can be written in 3D discrete time state space

form. Defining three states at discrete time k : $x_1(k) = d_i$, $x_2(k) = d_{i+1}$, $x_3(k) = d_{i+2}$. then if a unit discrete time increment represents the time the sensor head rotates through the angle γ :

$$\begin{bmatrix} x_1(k+1) \\ x_2(k+1) \\ x_3^-(k+1) \text{ or} \\ x_3^+(k+1) \end{bmatrix} = \begin{bmatrix} x_2(k) \\ x_3(k) \\ f^-(x_1(k), x_2(k), x_3(k), \gamma) \text{ or} \\ f^+(x_1(k), x_2(k), x_3(k), \gamma) \end{bmatrix} \quad (4)$$

i.e:

$$\mathbf{x}^\pm(k+1) = \mathbf{F}^\pm(\mathbf{x}^\pm(k)) \quad (5)$$

where \mathbf{F}^\pm is the non-linear function of the state $\mathbf{x}(k)$ according to each function $f^\pm(\dots)$, defined in equations 2 and 3. The superscripts \pm will now be dropped.

The above system model corresponds to the temporal relationship between past sensor measurements and the present range limits $x_3^\pm(k+1)$ within which $x_3(k+1)$ (or d_{i+3}) is bounded if it is assumed to belong to the contour being tracked.

4.2 Sensor Measurement Noise

The observation of the state is the range measurement $z(k)$, recorded just before prediction takes place:

$$z(k) = d_{i+2} = \mathbf{C}\mathbf{x}(k) + w(k);$$

$$\begin{bmatrix} 0 & 1 & 0 \end{bmatrix} \begin{bmatrix} x_2(k) \\ x_3(k) \\ f^-(x_1(k), x_2(k), x_3(k), \gamma) \text{ or} \\ f^+(x_1(k), x_2(k), x_3(k), \gamma) \end{bmatrix} + w(k)$$

where $w(k)$ is a zero mean additive noise process, with unique known variance, accompanying each sensor range value [7].

4.3 Recursive EKF Formulation

The tool used to place the above predictor/observer equations into recursive form is the EKF. After filter initialization (recording d_0 , d_1 and d_2), filter prediction takes place such that²:

$$\hat{\mathbf{x}}(k+1 | k) = \mathbf{F}(\hat{\mathbf{x}}(k | k)) \quad (6)$$

where the terms follow the usual EKF notation [10]³

²During filter initialization, it is possible that lines AB and BE in figure 6 are almost perpendicular. This will cause the model to produce its next gate at $\pm 90^\circ$ meaning that the next range point will definitely lie within the acceptable bounds. This action is however correct, as subsequent range points are guaranteed to produce further gates at angles of magnitude $< 90^\circ$, making the filter adapt its curvature constraints to the true properties of the surface.

³No system model noise term is used here, since the algorithm is to find range points which fall outside the strictly defined smoothness constraints of the derived model.

To provide full recursive prediction and state update, the state error covariance matrix $\mathbf{P}(k+1 | k)$ must also be calculated. The usual EKF solution to this problem requires the linearization of \mathbf{F} about the previous state prediction $\hat{\mathbf{x}}(k | k)$ so that differences between predicted and actual states at time k , $\tilde{\mathbf{x}}(k)$, can be used to update the prediction of $\mathbf{P}(k+1 | k)$:

$$\mathbf{P}(k+1 | k) = \nabla \mathbf{F} \mathbf{P}(k | k) \nabla^T \mathbf{F} \quad (7)$$

where $\nabla \mathbf{F}$ is the Jacobian matrix of \mathbf{F} . The accuracy of the predicted error covariance matrix in equation 7 is dependent on the local linearity of the function $f^\pm(\dots)$ about the previous predicted values of $\hat{\mathbf{x}}(k | k)$. Problems of filter *bias* and *inconsistency* can result, depending on $f^\pm(\dots)$. A recent, alternative solution is the use of the *distribution approximation filter* (DAF), which has been shown to be more accurate than linearization, and avoids the necessity to calculate the Jacobian matrix $\nabla \mathbf{F}$ [11].

The important aspects of this EKF cycle are:

1. *Innovation*: The difference between the expected and actual sensor data. If:

$$\mathbf{C}\hat{\mathbf{x}}^-(k+1 | k) \leq z(k+1) \leq \mathbf{C}\hat{\mathbf{x}}^+(k+1 | k) \quad (8)$$

then all range measurements are validated and the innovation $v(k+1)$ is set to zero. Else:

$$v(k+1) = \min \left\{ \begin{array}{l} \mathbf{C}\hat{\mathbf{x}}^-(k+1 | k) - z(k+1) \\ z(k+1) - \mathbf{C}\hat{\mathbf{x}}^+(k+1 | k) \end{array} \right\} \quad (9)$$

2. *Variance of Innovation*:

$$s(k+1) = \sigma_r^2(k+1) + \mathbf{C}\mathbf{P}(k+1 | k)\mathbf{C}^T \quad (10)$$

where $\sigma_r^2(k+1)$ denotes the recorded range variance at time $k+1$ [7].

3. *Validation Gate*. The innovation and its variance are used to form a validation gate equation:

$$D(k+1) = v^2(k+1)s^{-1}(k+1) \quad (11)$$

The magnitude of which is used to detect features.

4. The normal *EKF cycle continues* until optimal full state vector update results such that $\hat{\mathbf{x}}(k+1 | k+1)$ and $\mathbf{P}(k+1 | k+1)$ are determined and the system is now in recursive form [10, 7].

5 Results

Range versus scan angle, taken from a full 2π rads sweep in an outdoor, built-up area is shown in figure 7. Surrounding the range data are plots of $x_3^\pm(k+1 | k+1) \pm 3\sqrt{s(k+1)}$, these corresponding to '3 sigma limits' surrounding the updated state estimates of the range

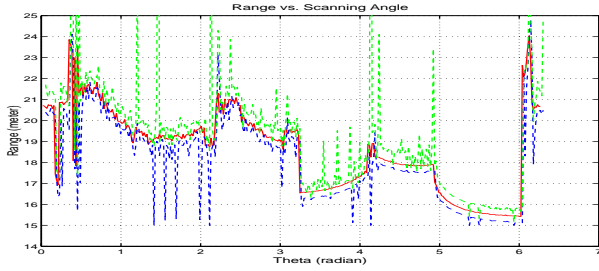


Figure 7: 3 sigma bounds and range readings when scanning a built-up area.

bounds (dashed lines) which enclose range data which results from surfaces with constant changes in spatial gradient, with 99.7% probability.

The peaks in the range bound curves result from combinations of d_i , d_{i+1} and d_{i+2} , which cause d_{i+3}^\pm to become singular⁴. Whenever the range curve exits the envelope of dashed lines, a feature is noted at that range point.

Figure 8 shows a zoomed view, from figure 7, of two walls between scan angles 4.1 and 6.1 rads. Changes in

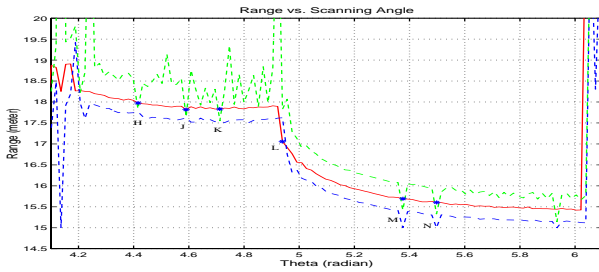


Figure 8: Zoomed view of a section of figure 8. The stars at H to N represent detected features.

smoothness have been detected at points H, J, K, L, M, and N. It can be seen in the right of the top graph that, with the exception of points M and N, the envelopes track the range values quite closely. If there was no noise in the measurements, the envelope would converge to the range values themselves, making the smoothness constraint on the surface being sensed, very stringent. In these experiments, the range measurements were accompanied by unique range variances, which cause the EKF cycle to be more lenient in its generation of the range bounds [12].

Figures 9 and 10 show similar results taken from a cliff face and cluster of trees. In figure 9, features are detected at the edges P and R, and along the surface at Q. The cluster of trees (figure 10) is a potential source of many features, based on changes in smoothness. Due to

⁴ when d_{i+3}^\pm in equations 2 and 3 are singular, the prediction lies on a line parallel to the next line-of-sight of the sensor so that they intersect at infinity. In this case, the range bounds lie on the minimum and maximum range of the sensor.

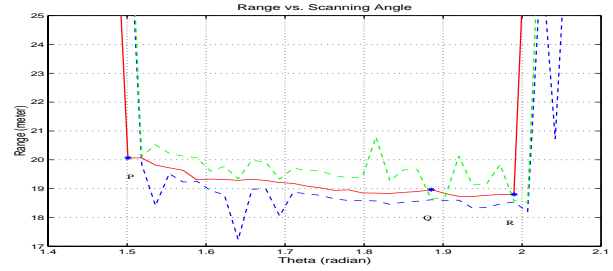


Figure 9: 3 sigma bounds and range data when scanning a cliff face. P to R are detected features.

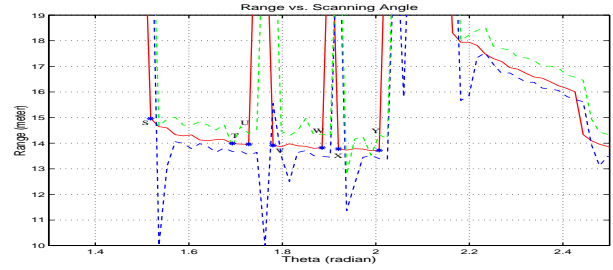


Figure 10: 3 sigma bounds and range data when scanning a cluster of trees. S to X are detected features.

the noise in the sensor measurements however, the filter cycle requires quite large changes in surface gradient, for feature detection (points S to Y).

The final test for any feature detection algorithm must lie in its ability to detect the same features from new positions. Figure 11 shows a plan view of a single 360° range scan and the range bounds in Cartesian coordinates. The lidar was mounted on a vehicle positioned at the triangle shown (coordinates (23, 15)). The scanned objects were: A: Tree cluster, B: Jagged rock face, C: Large circular enclosure and D: Brick wall. Features from the scan are shown as circles (○).

Finally, to show the success rate of feature detection repeatability from different sensor positions, figure 12 shows detected features from the same objects as figure 11, recorded from 5 different locations. Features are this time marked as stars (★), if they were successfully detected from all 5 positions. If they were detected from at least 2 positions they are marked as circles (○)⁵. Due to the statistical nature of the estimation process, not every feature is detected from all positions, but it can be seen that the algorithm has a reasonable success rate at finding the same feature form different positions. In the experiment conducted, 18 features could be detected from all 5 positions. This would provide an extremely useful fuel source for matching algorithms, on which mobile robot localization and map building could be based.

⁵ due to the finite resolution of the lidar, features were considered to coincide, if they were within a 1m distance of each other.

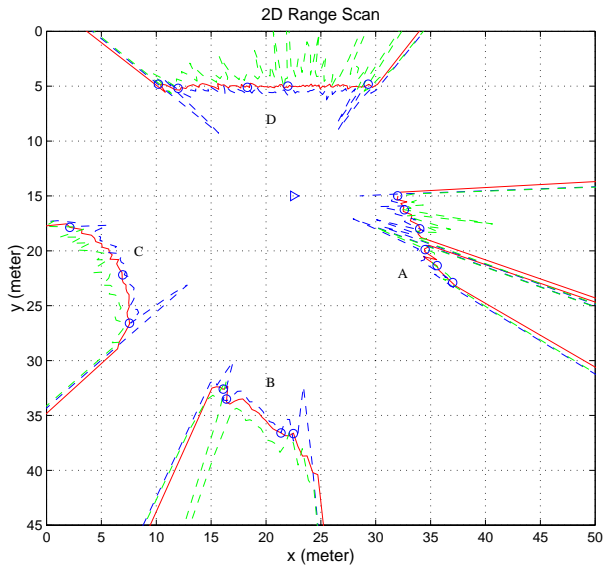


Figure 11: 3σ bounds and range readings when scanning a cluster of trees (at A), a jagged cliff face (at B), a large circular enclosure (at C) and a wall (at D). The circles represent detected features.

6 Summary

A feature detection algorithm has been derived and demonstrated which is specifically aimed at finding features from scanning range finders, on-line. This technique has the advantage of allowing all kinds of surfaces to be used for edge detection.

This ‘adaptive’ model was implemented in discrete time EKF recursive form, so that the effect of sensor measurement noise, when the range variances are known, on the detection of features is minimized. Results were demonstrated in which features were detected at relatively large distances ($> 10\text{m}$) with ladar range data in outdoor environments. Since the detector was successful at finding the same features from different sensor locations, the algorithm provides the potential for algorithms to match such features for navigation purposes in general outdoor environments.

Acknowledgments

GINTIC Institute of Manufacturing Technology, Singapore provided invaluable support for this work.

References

- [1] H. F. Durrant-Whyte. An autonomous guided vehicle for cargo handling applications. *Int. J. Robotics Research*, 15(5):407–440, 1996.
- [2] G. K. Schaffer, A. Stenz, W. L. Whittaker, and K. W. Fitzpatrick. Position Estimator for Underground Mine Equipment. Technical report, Carnegie Mellon University, Pittsburg U.S.A., 1990.

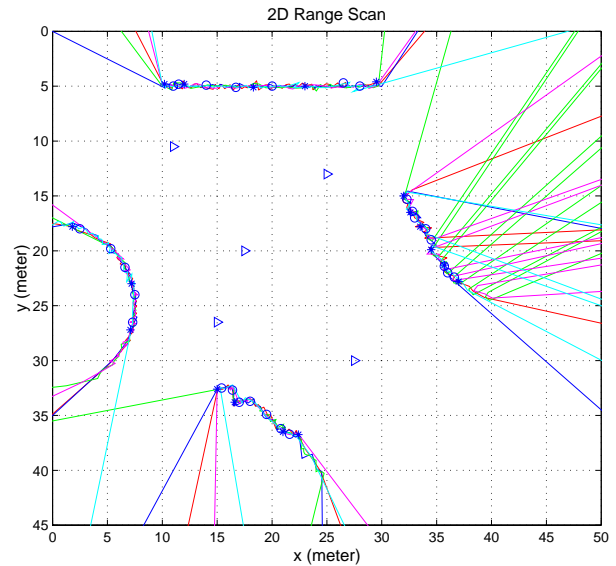


Figure 12: Detected features from several positions within the environment recorded in figure 12. The features marked as stars (\star) were successfully detected from all five positions, those marked as circles (\circ) were detected from at least 2 positions.

- [3] Wen Xu. Coherent source direction estimation for three-row bathymetric sidescan sensors. In *MITS/IEEE Oceans*, Seattle, USA, 1999.
- [4] J. Neira, J.D. Tardos, J. Horn, and G. Schmidt. Fusing range and intensity images for mobile robot localization. *IEEE Trans. Robotics and Automation*, 15(1), 1999.
- [5] John J. Leonard and Hugh F. Durrant-Whyte. *Directed Sonar Sensing for Mobile Robot Navigation*. Kluwer Academic Publishers, 1992.
- [6] Li Zhang and Bijoy K. Ghosh. Geometric feature based $2\frac{1}{2}$ d map building and planning with laser, sonar and tactile sensors. In *Int. Conf. Intelligent Robots and Systems*, 2000.
- [7] Martin D. Adams. *Sensor Modelling, Design and Data Processing for Autonomous Navigation*. World Scientific, 1999.
- [8] J. Borenstein, H. R. Everett, and L. Feng. *Navigating Mobile Robots: Sensors and Techniques*. A. K. Peters, Ltd., Wellesley, MA, 1995.
- [9] Berthold K.P. Horn. *Robot Vision*. M.I.T. Press, Cambridge Mass. U.S.A., 1986.
- [10] Y. Bar-Shalom and T.E. Fortmann. *Tracking and Data Association*. Academic Press, 1988.
- [11] S.J. Julier, J.K. Uhlmann, and H.F. Durrant-Whyte. A new approach for the nonlinear transformation of means and covariances in linear filters. *IEEE Trans. Automatic Control*, 1996.
- [12] M. D. Adams and A. Kerstens. Tracking naturally occurring indoor features in 2-D and 3-D with lidar range/amplitude data. *Int. J. Robotics Research*, 17(9):907–923, 1998.